Comparative kinetics study on carbonation of ettringite and meta-ettringite based materials

Bao Chen, Matthieu Horgnies, Bruno Huet, Vincent Morin, Kévyn Johannes, Frédéric Kuznik

Comparative kinetics study on carbonation of ettringite and meta-ettringite based materials

Bao Chen[1,2*], Matthieu Horgnies[2], Bruno Huet[2], Vincent Morin[2], Kévyn Johannes[1], Frédéric Kuznik[1]

[1] *Université de Lyon, CNRS, INSA-Lyon, Université Claude Bernard Lyon 1, CETHIL UMR 5008, F-69621, Villeurbanne, France*

[2] *LafargeHolcim Innovation Center, 95 rue du Montmurier BP15, 38291 Saint Quentin Fallavier, France*

* Corresponding author. E-mail address: bao.chen@insa-lyon.fr

Abstract

The use of ettringite-based materials for thermochemical heat energy storage has attracted researchers' attention in recent years since ettringite has advantages like low material cost and high energy storage density (~ 500 kWh/m^3). However, carbonation, which modifies its structure and reduces the capacity of energy storage, is an important hindrance to real applications. To address this issue, the present study focuses on the carbonation kinetics of three ettringite-based and corresponding meta-ettringite-based materials (dehydrated samples) exposed to different relative humidity (RH) and CO_2 concentrations. A mixture of 80 wt.% pre-blended Calcium Aluminate Cement / 20 wt.% OPC (C80P20) proved to be the most resistant against CO_2. The hydrated and dehydrated C80P20 grains carbonated slowly at 50 % RH and 1 vol.% CO_2, consuming little ettringite after 28 days. At 90 % RH, carbonation was accelerated such that all ettringite and meta-ettringite materials were depleted at 11 days with vaterite and aragonite as the main calcium carbonates. The produced $CaSO_4$ hydrates were found as hemihydrate at 70 % RH and gypsum at 90 % RH. Finally, the thermal energy storage capacity (TESC) of the material was systematically quantified as essentially decreasing with the carbonation degree of ettringite-based materials.

Key words: Carbonation durability, Ettringite-based materials, Meta-ettringite, Thermal energy storage

Cement chemist notation

A	Alumina (Al_2O_3)
C	Lime (CaO)
$\bar{C}$	Carbon dioxide (CO_2)
H	Water (H_2O)
M	Periclase (MgO)
S	Silica (SiO_2)
$\bar{S}$	Sulphur trioxide (SO_3)

Nomenclature

a	Weight percentage (%)
d	Mean diameter of pores (µm)
I	CO_2 binding quantity (g CO_2 / g anhydrous mixture)
I_0	Initial CO_2 binding quantity (g CO_2 / g anhydrous mixture)
I_{max}	CO_2 binding capacity (g CO_2 / g anhydrous mixture)
I_r	Absolute CO_2 binding quantity (g CO_2 / g anhydrous mixture)
I_t	Instant CO_2 binding quantity (g CO_2 / g anhydrous mixture)
k_0	Surface carbonation reaction rate constant
M	Molar mass (g / mol)
m	Weight (g)
P_{CO2}	Partial pressure of CO_2 (Pa)
P_{H2O}	Partial pressure of water vapour (Pa)
p	Porosity (vol. %)
R	Ideal gas constant
S_l	Liquid saturation degree (%)
T	Temperature (K)
t	Time (h)
X	Recalculated percentage of components in XRD (%)
X_{XRD}	Original component weight percentage from XRD analysis (%)
x	Carbonation degree (%)
ρ	Mass density (g / cm^3)

32 **Abbreviation**

BCSAF	Pre-blend of Belite-Calcium Sulphoaluminate-Ferrite Cement and anhydrite
p-CAC	Pre-blend of Calcium Aluminate Cement and calcium sulphate
CSA	Calcium Sulphoaluminate Cement
CSH	Calcium Silicate Hydrate
DSC	Differential scanning calorimetry
Deh	Dehydrated
Hc	Hemicarboaluminate
Hy	Hydrated
MIP	Mercury Intrusion Porosimetry
Monosulfate	Monosulfoaluminate
OPC	Ordinary Portland Cement
RH	Relative humidity (%)
TESC	Thermal energy storage capacity
TGA	Thermo-gravimetric analysis
w/c	Water to cement weight ratio
w/s	Water to solid ratio
wc.%	Weight fraction recalculated based on anhydrous cement mixture for XRD
XRD	X-ray diffraction analysis
XRF	X-ray fluorescence analysis

33

1. Introduction

Calcium trisulphoaluminate hydrate, also known as ettringite, is a promising thermal energy storage material due to its high energy density (~ 500 kWh/m^3), low working temperature (~ 60 °C), and wide availability as a cement hydration product [1–5]. Other cementitious materials, like gypsum (99 kJ/mol, ~ 200 °C) [6] and portlandite (104 kJ/mol, ~ 420 °C) [7], are limited by their low enthalpies and high working temperatures for energy storage. Recent reports on Calcium Sulfoaluminate Cement (CSA) show potential for application in thermal energy storage [4, 8–10] using their intrinsic high content of ettringite after hydration. One of the most important obstacles to application is its poor carbonation resistance [2], as being alkaline after the hydration of cement, these ettringite-based materials can even react with atmospheric CO_2 (~ 0.04 vol.%). Beside CO_2 concentration, the testified essential factors on carbonation durability include water to cement weight ratio (w/c), curing, cement dosage, type of cement, relative humidity (RH), temperature etc. [11–14].

Most investigations of carbonation kinetics concern Ordinary Portland Cement (OPC) based materials. Papadakis et al. [15] indicated that the carbonation of hydrated OPC decreases the pH of pore solution from more than 12.5 to below 9 (as low as 8.3). This neutralised solution then accelerates the dissolution of calcium and hydroxide ions from solid phases, thereby leading to mineralogical and microstructural modifications [11]. Likewise, carbonation processes tend to not only modify the porosity and microstructure of the samples, but also their mechanical performances and durability [12]. Carbonation reactions of the main minerals from hydrated OPC are listed in Table 1.

Table 1. Carbonation reactions of main minerals in hydrated OPC cement adapted from [12]

Components	Chemical formula	Carbonation reaction
Portlandite	$Ca(OH)_2$	$Ca(OH)_2 + CO_2 \rightarrow CaCO_3 + H_2O$
Calcium silicate hydrate	$(CaO)x(SiO_2)y(H_2O)z$	$(CaO)x(SiO_2)y(H_2O)z + xCO_2 \rightarrow xCaCO_3 + ySiO_2 \cdot tH_2O + (z - t)\ H_2O$
Tricalcium silicate	$3CaO \cdot SiO_2$	$3CaO \cdot SiO_2 + 3CO_2 + nH_2O \rightarrow 3CaCO_3 + SiO_2 + nH_2O$
Dicalcium silicate	$2CaO \cdot SiO_2$	$2CaO \cdot SiO_2 + 2CO_2 + nH_2O \rightarrow 2CaCO_3 + SiO_2 + nH_2O$
Ettringite	$3CaO \cdot Al_2O_3 \cdot 3CaSO_4 \cdot 32H_2O$	$3CaO \cdot Al_2O_3 \cdot 3CaSO_4 \cdot 32H_2O + 3CO_2 \rightarrow 3CaCO_3 + 3CaSO_4 \cdot 2H_2O + Al_2O_3 \cdot xH_2O + (26 - x)H_2O$
Monosulfoaluminate	$3CaO \cdot Al_2O_3 \cdot CaSO_4 \cdot 12H_2O$	$3CaO \cdot Al_2O_3 \cdot CaSO_4 \cdot 12H_2O + 3CO_2 \rightarrow 3CaCO_3 + CaSO_4 \cdot 2H_2O + Al_2O_3 \cdot xH_2O + (10 - x)H_2O$

Nishikawa et al. [16] and Grounds et al. [17] proposed carbonation kinetics models for ettringite based on powder samples at RH superior to 95 % with 5 vol.%, and atmospheric CO_2, respectively. Although they hold different opinions, both agree that the diffusion of CO_2 in the particles plays a significant role during carbonation. Detailed numerical work from Chen et al. [18] pointed out the influence of temperature, water vapour pressure, and CO_2 pressure on the carbonation of ettringite powder through **Eq. 1**, where x is the degree of carbonation (%), k_0 is the surface carbonation reaction rate constant, P_{H2O} (Pa) and P_{CO2} (Pa) are partial pressure of water vapour and CO_2, respectively. Moreover, the process of dissolution of gaseous CO_2 into water was defined as the rate limiting step [18].

$$v = \frac{dx}{dt} = k_0 e^{39907/RT} \cdot P_{H2O} \cdot P_{CO2} \quad \textbf{(Eq. 1)}$$

Zhou and Glasser [19] investigated the carbonation on ettringite powders and pellets (~ 2.5 mm thick) compacted to 80 % theoretical density, to determine the effect of form. They confirmed the impact of temperature and RH as reported in [18]. Monosulfoaluminate (monosulfate) was found inside pellets since the insides retain water, leading to recrystallisation [19]. Besides, hemihydrate ($CaSO_4 \cdot 0.5H_2O$) and gypsum ($CaSO_4 \cdot 2H_2O$) were both detected as calcium sulphate hydrates after the carbonation of ettringite pellets [19]. The calcium carbonate polymorphs are vaterite [16,19] and aragonite [16]. According to Pajares et al. [20], $Ca(OH)_2$ is able to delay ettringite carbonation process because of its higher reaction rate with CO_2.

Instead of using pure ettringite, Ndiaye et al. [4] investigated the carbonation effects of ettringite-enriched CSA cement paste powder under 4 vol.% CO_2 and 65 % RH at 25 °C. The researchers observed hemihydrate instead of gypsum, aragonite and vaterite as carbonate phases, but no monosulfate. Mechling et al. [13] found that the calcium sulphate was gypsum and depths of carbonation increased when the w/c ratio was raised, which is consistent with [21]. Furthermore, carbonation kinetics seems closely related to the porosity controlled by the w/c ratio [13]. Ioannou et al. [22,23] added that the dense microstructure of blended CSA cement did not largely impact carbonation resistance. However, additives like slag, fly ash [21], and polymers [24] could decrease carbonation rates. Hargis et al. [14] concluded that the rise of anhydrite content could lead to faster ye'elimite hydration, thereby increasing carbonation resistance. Zhang and Glasser [25] assumed that a partially carbonate-substituted ettringite persisted near the surface of CSA cement based concrete after natural carbonation of

16 years. This compound could be part of the CO_3-SO_4- ettringite solid solution series as reported in [26–28].

However, to the authors' knowledge, there is no data available on carbonation of meta-ettringite and meta-ettringite-based materials. Therefore, new investigations are necessary to evaluate the carbonation kinetics of ettringite- and meta-ettringite-based materials, particularly if they are used in energy storage system with circulation of air. Except the more severe carbonation issue [22,23,29], CSA cement is inferred to be an alternative to OPC, owing to similar mechanical performance but lower CO_2 emission for production [30]. Thus, a blended mixture composed of OPC and Calcium Aluminate cement blended with calcium sulphate is an interesting possibility for improving mechanical properties of hydrated cement paste, while possessing high ettringite content. In this study, and with the specific aim at analysing the use of industrial cements, three blended cements were used to investigate the carbonation kinetics of ettringite and meta-ettringite that are supposed to be the major phases in hydrated and dehydrated cement pastes, respectively—i) Two made from the mixture of OPC and pre-blended Calcium Aluminate Cement containing calcium sulphate (p-CAC), and ii) A pre-blended Belite-Calcium Sulfoaluminate-Ferrite Cement containing anhydrite (BCSAF). The experiments were completed under ambient conditions (20 °C, 50 % RH, 0.04 vol.% CO_2) and accelerated carbonation (1 vol.% CO_2) with various RH at 20 °C. After the experiments, all samples were analysed using Thermo-gravimetric analysis (TGA) and X-ray diffraction (XRD) to quantify bound CO_2 and evolution of mineral components.

2. Materials and methods

2.1. Materials

High calcium aluminate cements containing additional calcium sulphate (p-CAC and BCSAF) were used to obtain pastes rich in ettringite. To produce pastes with different ettringite contents, some p-CAC was mixed with OPC (CEM I 52.5 N), improving mechanical properties and decreasing the risk of self-breakage due to significant shrinkage. The BCSAF was light brown cement with high ye'elimite content. Chemical compositions and mineralogical phases of the three cements were analysed by X-ray fluorescence (XRF) and XRD, and are shown in Table 2. Minor oxides and mineralogical phases were not listed, resulting in total values less than 100 %.

Table 2. Percentages (wt.%) of chemical and mineralogical compositions of cements used

	OPC	p-CAC	BCSAF		OPC	p-CAC	BCSAF

SiO_2	20.25	1.87	12.42	C_3S	70.7	-	-
Al_2O_3	5.44	23.43	16.87	C_2S	7.3	-	30.9
Fe_2O_3	2.48	0.47	6.25	C_4AF	7.4	-	16.4
CaO	64.25	43.17	47.33	C_3A	8.5	-	-
MgO	1.17	0.26	1.44	$C\bar{S}H_{0.5}$	3.2	-	3.7
K_2O	0.22	0.14	0.67	$C\bar{S}H_2$	2.6	-	1.2
Na_2O	0.18	0.05	0.09	$C\bar{S}$	-	52.5	10.7
SO_3	3.33	28.78	9.94	$C_{12}A_7$	-	3.5	-
TiO_2	0.15	1.12	0.88	$C_4A_3\bar{S}$	-	-	31.1
Mn_2O_3	0.10	<0.05	0.06	MgO	-	-	0.5
P_2O_5	0.26	0.05	0.06	Ferro-perovskite	-	-	3.6
Cr_2O_3	<0.05	<0.05	<0.05	Ettringite	-	-	1.5
ZrO_2	<0.05	<0.05	<0.05	Monosulfate	-	-	0.3
SrO	0.06	<0.05	0.13	Amorphous phase	-	44.0	-
Total	97.99	99.54	96.24		99.7	100.0	99.9

2.2. Preparation of samples

The p-CAC was manually mixed with 20 wt.% and 40 wt.% of OPC in order to prepare samples with different levels of ettringite. The BCSAF was prepared without any other cement. To obtain high porosities [31], demineralised water was used with water to solid ratio (w/s) of 1.1 to hydrate three binders by a VMI/Rayneri mixer at 700 r/min for 3 minutes, then at 1000 r/min for 10 minutes. Before the addition of the blend into demineralised water, a small quantity (0.05 wt.% of blend) of Chryso® Premia 162 was pre-introduced to the water to assure good workability retention. After the addition of cement mixtures, a certain amount of Kelco-Crete® DG-F (0.1 wt.% of water) was added slowly to prevent agglomeration. The used formulas for the different mixtures are summarised in Table 3. The cementitious pastes were then poured into polystyrene moulds (4 × 4 × 16 cm^3) and covered by a glass plate sealed with rubber for 24 h. After that, the samples were demoulded and stored in sealed bags for hydration of 28 days (1 day in moulds and 27 days in sealed plastic bags) at ~ 22°C. In parallel with the preparation of prisms for grains, the same mixtures (3 prisms for each) were also cast for compression strength test.

Table 3. Mixture designs for different pastes preparation of 800 cm^3

Samples	Main cement (g)	OPC (g)	Chryso® Premia 162 (g)	Kelco-Crete® DG-F (g)	Demineralised water (g)
BCSAF	563.3 (BCSAF)	/	1.14	0.620	618.8
C80P20	451.0 (p-CAC)	112.8	1.14	0.620	619.3

C60P40	342.2 (p-CAC)	223.2	1.14	0.622	621.3

After 28 days of curing, the prisms were ground in a porcelain mortar with a pestle and passed through sieves of different sizes to collect 1–2 and 2–4 mm grains. Grains were then sealed in vacuumed plastic bags for later experiments. The hydration of samples was not stopped by organic solutions, to approximate a real-world scenario for energy storage.

2.3. Accelerated and natural carbonation methods

Approximately 150 g of paste of each grain size was oven-dehydrated at 90 °C for 2 days to obtain meta-ettringite-based materials. Approximately 4 g of sample per study case was tiled as a monolayer in an 8 cm aluminium dish. The dehydrated samples as well as corresponding original hydrated cement samples (1–2 and 2–4 mm) made of the three mixtures listed in Table 3 were then carbonated in a CO_2 chamber (Pharma 600 of Weisstechnik®) at 20 °C, 1 vol.% CO_2, and respective RH (50 %, 70 %, and 90 %) for different periods from several hours to 28 days. The particle sizes and RH were set with respect to the internal conditions of an energy storage system. The effect of RH was studied for each case using non-hydration-stopped samples. As a reference, the same prepared samples sustained natural carbonation in an environmentally controlled chamber (50 % RH, 20 °C, and ~ 0.04 vol.% CO_2) for 0, 11 days, 1, 2, 3, and 6 months.

2.4. Characterisation methods

Before experiments on carbonation, compression strength tests (RP 12/50/300 FCC of 3R®) were executed on 3 prims ($4 \times 4 \times 16$ cm^3) for each hydrated binder after 7 and 28 days of curing. Mercury Intrusion Porosimetry (MIP), granulometry, and isotherm absorption were also performed on small pieces and grains of materials at 28 days. After each interval of carbonation, the specimens were ground to a powder (< 100 µm) and characterised by TGA and XRD.

2.4.1. Thermal characterisation

TGA (Mettler TGA-DSC 3^+) was principally used to quantify the carbonates. An approximately 40 mg sample was added to the device and heated from 30 to 1000 °C at 10 °C/min under a nitrogen flow of 20 mL/min. For cement pastes hydrated by a high w/c ratio, there existed an overlap between weight loss of combined water and CO_2 at 450–550 °C [32]. The range of decarbonisation temperature was thus defined between 550 and 1000 °C. The error in the TGA measurement was approximately 1 %. Due to the bound water release

into gas phase as water vapour and weight loss of samples through carbonation experiments, the indicator of carbonation was calculated by normalizing the CO_2 mass gain by the anhydrous content (**Eq. 2**):

$$I = \frac{m_{CO2}}{m_{anhydrous\ blend}} = \frac{m_{initiale\ TGA} * (a_{550\ °C} - a_{1000\ °C})}{m_{initiale\ TGA} * a_{1000\ °C}} \qquad \textbf{(Eq. 2)}$$

Where I is the CO_2 binding quantity (g CO_2 per g anhydrous mixture), m (mg) is the weight from TGA, and *a* (%) is the weight percentage from TGA.

When preparing the samples, carbonation was hard to avoid. The absolute CO_2 binding quantity (I_r) during experiments was then defined as the difference between the CO_2 binding quantities at each carbonation date (I_t) and at time zero (I_0) in **Eq. 3**:

$$I_r = I_t - I_0 \qquad \textbf{(Eq. 3)}$$

To determine thermal energy storage capacity (TESC), the carbonated grain samples were powdered and characterised by TGA-DSC (Sensys Evo TG-DSC), which provided thermal analysis simultaneous with the loss of weight. Approximately 10 mg of specimen was heated at 80 °C for 5 h with a speed of 10 °C / min from 25 to 80 °C, while the sample was protected by a nitrogen flow of 50 mL / min. Thermal analysis data were acquired by Calisto Acquisition and processed by Calisto Processing (both software) to give loss of weight and enthalpies. The systematic uncertainty in enthalpy measurement was approximately 1 %.

2.4.2. XRD

The XRD method used was a semi-quantitative analysis, for not only the mineralogical variation but also mass fraction changes during carbonation. The XRD device used a Philips/PANalytical X'Pert Pro-MPD Powder Diffractometer with an X'Celerator detector of incident CuKα radiation beam by 40 kV and 40 mA to a rotation sample. The specimens were scanned for 40 minutes from 2θ = [5–65 °] by a step of 0.25 ° without protection from CO_2. For dehydrated specimens, the quantity of meta-ettringite was calculated with a nora 35 rutile standard using the external standard method for BCSAF cases and nora 35 for the other two mixtures. Although the semi-quantitative analysis of amorphous meta-ettringite and CSH phases was not accurate for the amounts but the trends of quantity evolution could still be traced.

For the variation of mass caused by water loss during carbonation, the semi-quantitative results were deemed not comparative for different carbonated samples. Hence, the analytical results were recalculated with TGA results (**Eq. 4**).

$$X = \frac{X_{XRD} * m_{initial\,TGA}}{m_{anhydrous\,blend}} \times 100\,\% = \frac{X_{XRD} * m_{initial\,TGA}}{m_{initial\,TGA} * a_{1000°C}} \times 100\,\% = \frac{X_{XRD}}{a_{1000°C}} \times 100\,\% \qquad \textbf{(Eq. 4)}$$

Where X (wc.%) is the recalculated percentage of components relating to the mass of anhydrous blend, X_{XRD} (%) the original component weight percentage from XRD analysis, *m* (mg) and *a* (%) are the weight and weight percentage from TGA, respectively. X can exceed 100 % for several components of high content.

2.4.3. Theoretical CO_2 binding capacity by XRF

According to [14], the theoretical CO_2 binding capacity (I_{max}, g bound CO_2 / g anhydrous cement) of an anhydrous cement could be approximately inferred from the quantity of its main carbonatable oxides from XRF results (see **Eq. 5**) with two assumptions. 1) The sulphate ion only exists in calcium sulphate after a total carbonation of cement pastes, and 2) CaO and MgO are the main carbonated phases.

$$I_{max} = \frac{m_{CO2}}{m_{anhydrous\,mixture}} = \frac{\left(\frac{a_{CaO}}{M(CaO)} + \frac{a_{MgO}}{M(MgO)} - \frac{a_{SO3}}{M(SO3)}\right) * m_{cement} * M(CO_2)}{m_{anhydrous\,mixture}} \qquad \textbf{(Eq. 5)}$$

Where m (mg) is the weight from TGA, *a* (%) is the weight percentage in XRF, and M is the molar mass.

2.4.4. Granulometry

Granulometry was executed on collected grains by stereoscopic magnifier STEMI SV 11 with a Zeiss electronic fibre optic lighting KL 1500. The 1–2 and 2–4 mm particles were randomly picked for optical observation. After observation of each sample, the Olympus Image Analysis Software carried out measurement for each grain. The approximate maximum and minimum values of 10–30 grains were used to calculate the mean diameter.

2.4.5. MIP

MIP tests were carried out on small pieces from prims of hardened pastes of 28 days (4 × 4 × 16 cm^3) using an Autopore IV (Micromeritics, USA). Before testing, samples were dried in an oven at 45 °C overnight. The suggested contact angle for ordinary cement pastes [31] was presumed to be 130 °. On this basis, the pressures used enabled a pore diameter coverage of approximately 3 nm–360 µm.

2.4.6. Water isotherm absorption

Six samples of 10 g each from the three binders' grains of both sizes were oven dried at 40 °C to extract pore water with soda lime protection for 10 days. Then, each dried sample was separated to 3 samples of approximately 2 g (18 samples in total) and exposed in hermetic chambers at 20 °C under soda lime protection. The RH in chambers were controlled by saturated salts solutions and an internal air circulation, typically $Mg(NO_3)_2$ for 55 % RH, NaCl for 75 % RH, and KNO_3 for 95 % RH [33]. The variation of weight was recorded every week until stable (< 0.1 wt.%). Therefore, liquid saturation degree (S_l) in per gram dry sample is expressed as **Eq. 6**:

$$S_l = \frac{m \cdot \rho_{dry\ sample}}{p \cdot \rho_{water}} \times 100\ \% \quad \textbf{(Eq. 6)}$$

Where, m is absorbed water mass (g per g dry hydrated sample), $\rho_{dry\ sample}$ is the dry material density (g·cm^{-3}), p is the porosity (vol. %), and ρ_{water} is the liquid water density.

3. Results

3.1. Characterisation of reference materials before carbonation

The physical characteristics of the hardened mixtures are summarised in Table 4 using methods like theoretical CO_2 binding capacity, water vapour isothermal absorption, MIP, and compressive strength. The grains of different mixtures were generally in the 1–2 mm and 2–4 mm ranges. For C80P20, the mean size was 1.04 mm for 1–2 mm, while it was 2.07 mm for 2–4 mm. Similarly, it was 0.98 mm and 2.50 mm for 1–2 mm and 2–4 mm of C60P40, respectively, 1.13 mm and 2.11 mm for BCSAF. The compressive strengths generally increase with curing time and are the order C80P20 > C60P40 > BCSAF. According to **Eq. 5**, theoretical CO_2 binding capacities are approximately 0.25, 0.32, and 0.29 for anhydrous mixtures C80P20, C60P40, and BCSAF, respectively. For each hydrated binder, the quantity of absorbed water vapour at 20 °C increases with the rise of RH. Grains of size 2–4 mm get a higher content of absorbed water vapour than those of 1–2 mm. However, the total absorbed water content for all grains is not significant. Because of their high w/c ratios, the hydrated binders possess porosities 34 %, 38 %, and 54 % for C80P20, C60P40 and BCSAF, respectively. For hydrated mixtures, most pores are in the 0.03–1 µm range and they get less porosity from micro-pores with diameters smaller than 0.01 µm, or pores with diameters larger than 1 µm (Fig. 1). No significant pore volume having a mean diameter greater than 0.3 µm is observed. However, BCSAF has the most significant pore volume with a diameter less

than 0.1 µm, followed by C60P40, and very few for C80P20. After being dried at 90 °C for two days, the total porosities of C80P20 and C60P40 go up, but the volume of pores of each range also gets bigger. The pore volume for dehydrated C80P20 increases to 41 % and is mainly impacted by pores < 0.03 µm and 0.1 < d < 0.3 µm. Dehydrated C60P40 and BCSAF have pore volume rise in all size ranges of pores and they hold similar general pore volume of approximately 55 %. Table 5 gives the original mineralogical compositions in the samples before carbonation experiments (measurements done by XRD).

Table 4. Physical characteristics for three hardened mixtures*

	Experimental conditions		C80P20	C60P40	BCSAF
Theoretical CO_2 binding capacity [g CO_2 / g anhydrous mixture]	Calculation		0.25	0.32	0.29
Water vapour absorption [wt.% by dry hydrated sample]	55 (5) % RH	1–2 mm	0.27	0.34	0.54
		2–4 mm	0.59	1.02	0.76
	75 (5) % RH	1–2 mm	0.48	0.67	0.88
		2–4 mm	0.83	1.23	1.05
	95 (5) % RH	1–2 mm	2.50	3.88	2.40
		2–4 mm	2.54	3.71	2.68
Total porosity at 28 days (using MIP) [vol.%]	Hydrated (ettringite-based)		34	38	54
	Dehydrated (meta-ettringite-based)		44	54	54
Compressive strength [MPa]	Hydrated pastes at 7 days		14.9 (0.8)	10.2 (0.6)	7.1 (0.3)
	Hydrated pastes at 28 days		15.8 (1.0)	12.0 (0.6)	9.0 (0.6)

* The values in parentheses present uncertainty of measurements.

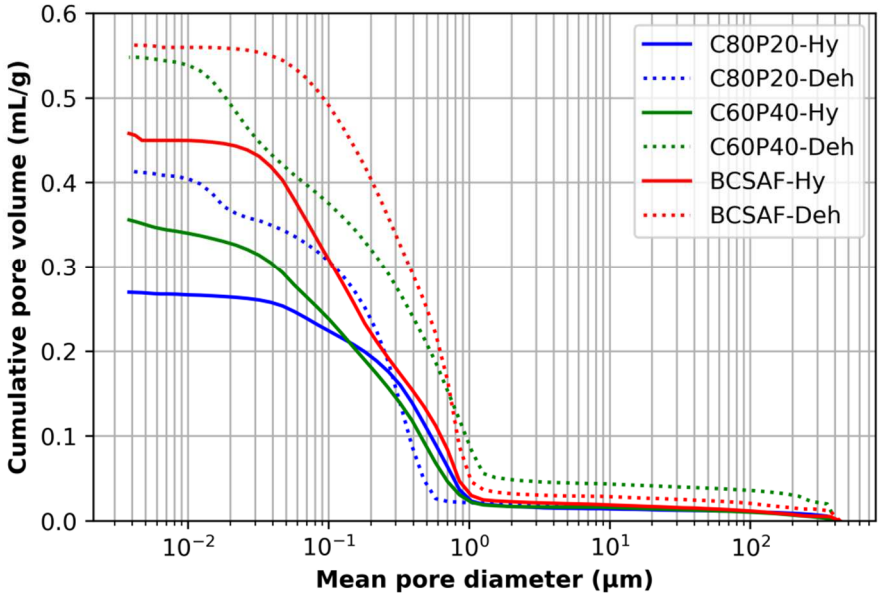

Figure 1. Cumulative pore volume of each hydrated and dehydrated pastes, measured by MIP

Table 5 Original mineralogical compositions in XRD of hydrated and dehydrated samples basing on three binders used before carbonation test*

	C80P20		C60P40		BCSAF	
	Hydrated	Dehydrated	Hydrated	Dehydrated	Hydrated	Dehydrated
C_2S	0.9	1.5	0.8	0.5	5.1	2.3
Monosulfate (12 H_2O)	0.3	1.2	5.8	2.2	3.1	1
Ettringite	75.3	/	67.6	/	45.6	/
Strätlingite	19.3	24	/	/	12.3	7.5
Katoite	/	/	/	/	11.3	14.3
Iron rich siliceous hydrogarnet	/	/	9.8	6.1	18.6	21.3
Monocarbonate	/	/	/	/	0.5	15.4
Hc	0.4	7.6	8.9	18.1	0.8	7.5
Calcite	/	/	1.6	0.2	2.8	0.9
Gypsum	/	/	2.7	3.1	/	/
AH_3	3.7	9.4	/	13.7	0.2	2.4
Amorphous phase	/	56.2	/	56.3	/	29.8

* The components less than 1 % could be neglected in this study.

3.2. Carbonation results of three binders by TGA

Fig. 2 shows accelerated carbonation results at 70 % RH and 1 vol.% CO_2 by TGA for the three mixtures of 2–4 mm in different hydration states. Note that t = 0 is noted as t = 0.01 [h] in the graphs with a logarithmic scale. For hydrated samples (Fig. 2 a), the slope break points of curves are at 6 h for BCSAF and 24 h for C60P40, while for dehydrated samples (Fig. 2 b)

they are at 6 h for BCSAF and 2 h for C60P40 with respect to 24 h for C80P20 in both cases. Here, the slope break point of carbonation is defined as the point at which the slope of the curve changes significantly in a logarithmic scale plot. The hydrated samples demonstrate a generally larger CO_2 binding quantity and carbonation rate before 24 h than those of dehydrated grains. Specifically, the carbonation rates of dehydrated samples are so small that there is no difference for three binders during the first 2 h, and then the increase of rate is in the order of C60P40 > BCSAF > C80P20. Among them, the carbonation rate of dehydrated C60P40 exceeds even that of the hydrated samples. In fact, almost no water remains in the pores after dehydration. Therefore, it takes some time to absorb enough water and CO_2 to start carbonation. Generally, no obvious difference of CO_2 binding quantity between hydrated and dehydrated samples is observed. For all three samples, carbonation rate during 11 ~ 28 days reduced significantly even if the slope of the curve in logarithmic scale does not change with time. Especially for C60P40, the variation of carbonation degree is very small (~ 0.01). Differing from the other two binders, dehydrated C80P20 presents a high rate of carbonation after 11 days. At 11 days, carbonation degrees of hydrated samples reach values of 38 %, 60 %, and 52 % for C80P20, C60P40, and BCSAF, respectively, while for dehydrated samples, the corresponding values are 25 %, 60 %, and 56 %, respectively. Therefore, C80P20 possesses a higher resistance against CO_2 than the other two binders. Given this fact, only the results of C80P20 will be measured and discussed.

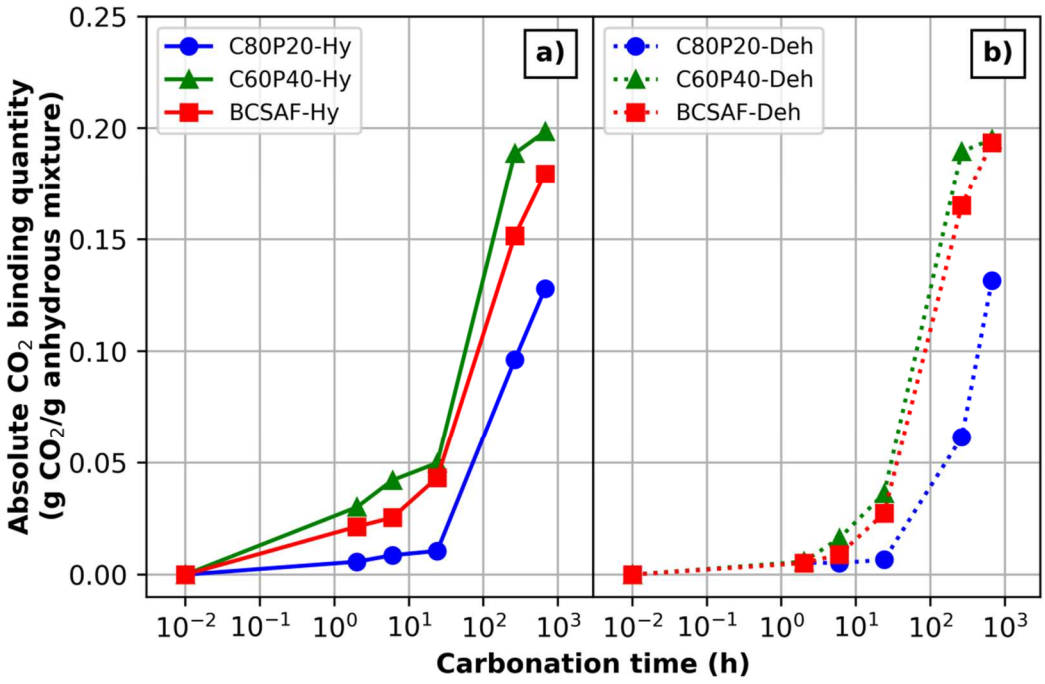

Figure 2. Absolute CO_2 binding quantity of hydrated a) and dehydrated b) cement pastes of C80P20, C60P40, and BCSAF of 2–4 mm, as a function of carbonation time at 70 % RH and 1 vol.%.

3.3. Detailed carbonation results of C80P20 by TGA

Fig. 3 shows the CO_2 binding quantity of hydrated and dehydrated C80P20 for both sizes of particles at different RH and CO_2 concentrations by TGA. Under 50 % and 90 % RH, the particle size effect is not visible for both states for each duration of carbonation. Under 70 % RH, the difference is more significant after 11 days of accelerated carbonation for both ettringite (~ 0.03) and meta-ettringite (~ 0.05) based cases.

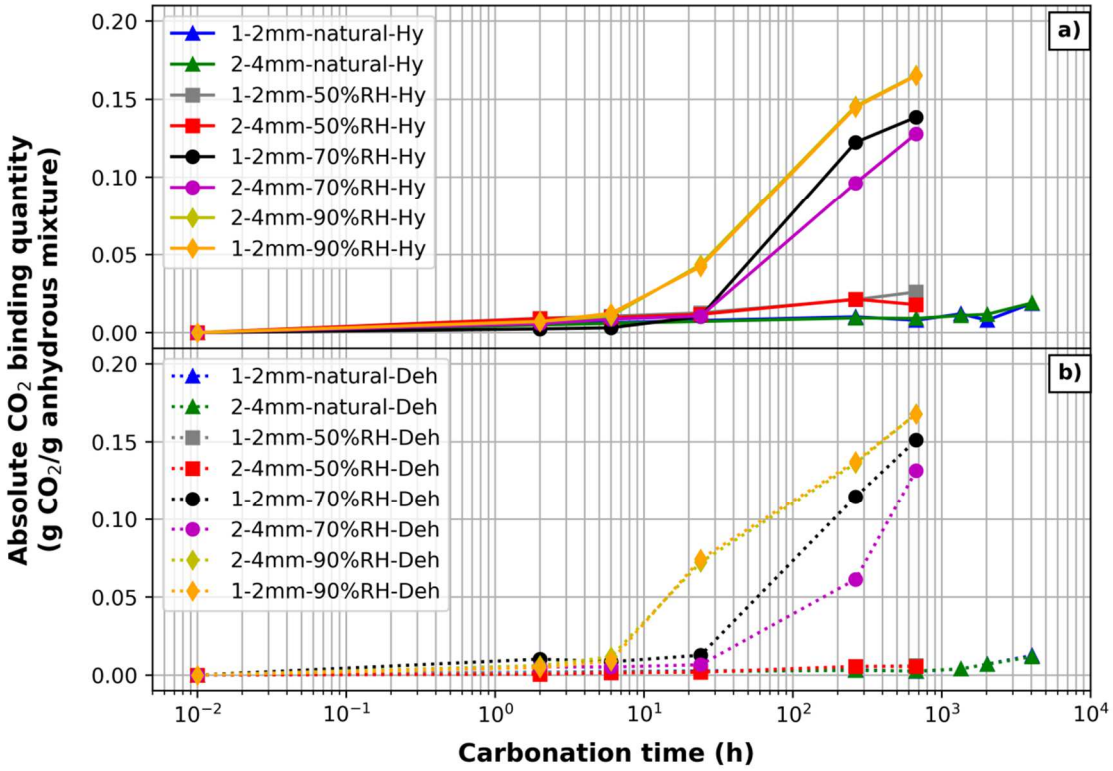

Figure 3. Absolute CO_2 binding quantity of a) hydrated and b) dehydrated C80P20 grains of 1–2 and 2–4 mm over carbonation time under natural conditions and accelerated conditions (at various RH and 1 vol.% CO_2)

For hydrated samples (Fig. 3 a), low RH appears to delay the carbonation. The accelerated carbonation of hydrated C80P20 at 50 % RH is very slow. After 11 days, the quantity of bounded CO_2 is approximately 0.02 g per g of anhydrous mixture. Moreover, under 50 % RH, the effect of CO_2 concentration on carbonation of the hydrated samples is not significant. The values of CO_2 binding quantity are 0.03 and 0.01 for accelerated and natural carbonation at 28 days, respectively. When RH increases to 70 %, the slope break point of the degree of

carbonation occurs at 24 h, when the quantity accumulation of absorbed CO_2 is very steep. At 28 days, the CO_2 binding quantities are almost the same (0.14 and 0.13) for both hydrated and dehydrated samples. Under 90 % RH, the slope break point advances to 6 h and the CO_2 binding quantity reaches 0.17 after 28 days of carbonation.

For dehydrated pastes (Fig. 3 b), the values of CO_2 binding capacity at 50 % RH are only 0.005 for accelerated carbonation and 0.003 for natural carbonation at 28 days, which are much smaller than those of hydrated specimens. Compared to hydrated samples, the dehydrated samples demonstrate the following approximate capacities for capturing CO_2 at 28 days—0.13–0.15 at 70 % RH and 0.17 at 90 % RH for both sizes of grains. Note that for the accelerated carbonation at 1 day under 90 % RH, the dehydrated samples of both sizes indicate a higher CO_2 binding quantity (0.072) than hydrated ones (0.044).

To summarise, a high CO_2 concentration has very little carbonation effect on dehydrated C80P20 samples under 50 % RH but has a more significant effect on hydrated ones. The carbonation rate increases steeply with RH going up. At 90 % RH, the curve profiles of the hydrated and dehydrated samples are alike, and show no effect of gain size.

3.4. Carbonation results of C80P20 by XRD

3.4.1. Accelerated carbonation at 50 % RH

Fig. 4 presents the evolution of phase assemblage by XRD as a function of carbonation time for the 2–4 mm C80P20 samples of different hydration states. In the following XRD results, the $CaCO_3$ and $CaSO_4 \cdot XH_2O$ present the total fraction of polymorphs of $CaCO_3$ and $CaSO_4 \cdot XH_2O$, respectively. The evolution of carbonate components is very slight for the grains in four cases. For hydrated C80P20 (Fig. 4 a), the quantity of ettringite decreases slightly, while some monosulfate forms at the very beginning with minor change as time progresses. Besides, a small amount of calcium hemicarboaluminate (Hc, $C_4A\bar{C}_{0.5}H_{12}$) is evidenced at an early stage of carbonation. During carbonation at 50 % RH, calcium carbonates are not visible.

For dehydrated samples (Fig. 4 b), Hc is formed after oven drying in the presence of fresh air flow and keeps a relatively high level, approximately 8 wc.%, over the experiments and tends to increase at 28 days. Calcium carbonates and calcium sulphate hydrates are not measurable in XRD even after 28 days of accelerated carbonation at 50 % RH. The reformation of ettringite progresses gradually to 14 wc.% at 28 days, while monosulfate

crystallises quickly during the initial hours and eventually stabilises at approximately ~ 8 wc.%.

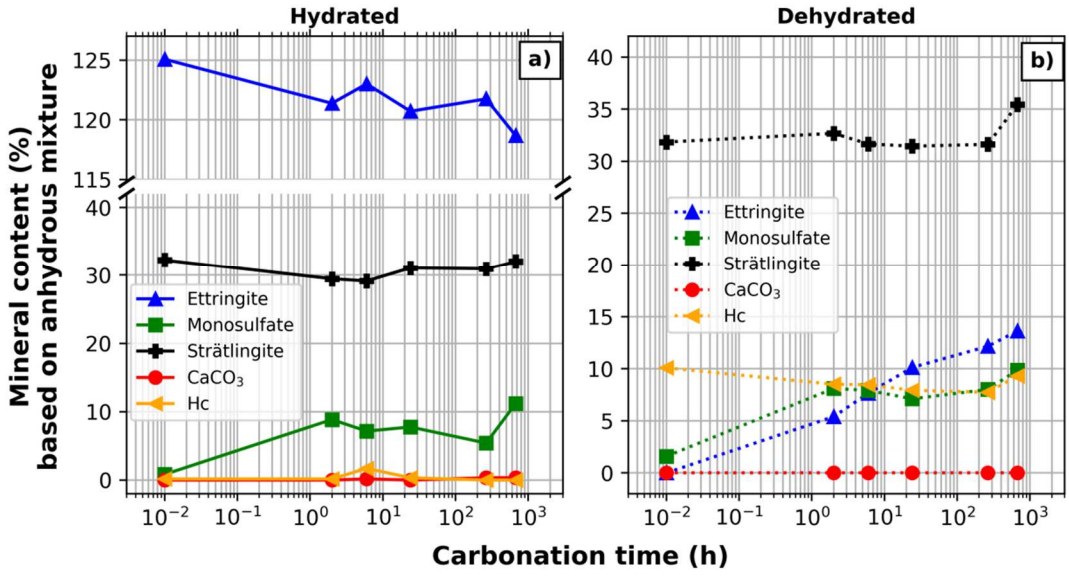

Figure 4. Calculated mineralogical contents in a) hydrated and b) dehydrated C80P20 of 2–4 mm after different periods of accelerated carbonation under 50 % RH and 1 vol.%

3.4.2. Accelerated carbonation at 70 % RH

According to TGA results (Fig. 3), accelerated carbonation under 70 % RH is significantly greater than it is under 50 % RH. For hydrated samples (Fig. 5 a)), the content of ettringite does not change during the first 24 h, but monosulfate rises to 11 wc.%. Ettringite is then substantially carbonated (55 % of total ettringite) during the following 10 days, accompanied by the depletion of all formed monosulfate. The carbonation process during this period produces 40 wc.% of $CaCO_3$ polymorph, which agrees well with the steep growth of CO_2 binding quantity in TGA at 11 days. All ettringite in the sample is consumed at 28 days, yielding approximately 54 wc.% of calcium sulphate hydrates. Strätlingite is not carbonated over carbonation time and tends to increase.

For dehydrated samples (Fig. 5 b), the presence of Hc after being dried in the oven is the same as in the 50 % RH case, before entirely carbonating after 24 h. The reformation of ettringite is more rapid than 50 % RH owing to more water vapour available under 70 % RH. However, the quantity of reformed ettringite only reaches 17 wc.% at 24 h. Afterwards, abundant $CaCO_3$ vaterite and aragonite are detected, while monosulfate and ettringite get

partly carbonated. Calcium sulphate, being proved as hemihydrate, grows sharply from 24 h. Given the small variation in quantity during the investigation, strätlingite is hardly carbonated. Besides, an increasing trend of strätlingite is found at 28 days of carbonation.

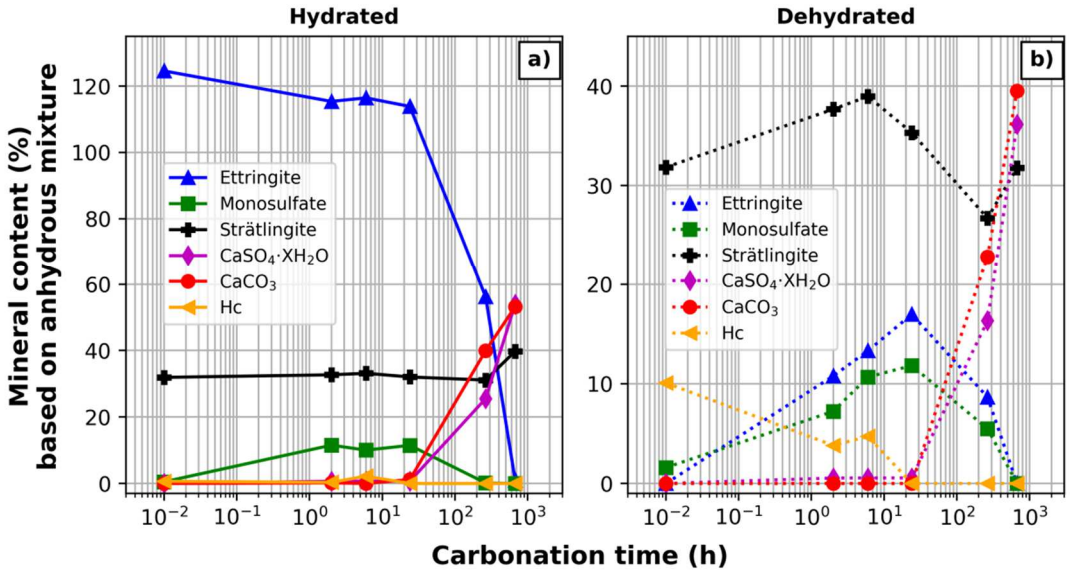

Figure 5. Calculated mineralogical contents in a) hydrated and b) dehydrated C80P20 of 2–4 mm after different periods of accelerated carbonation under 70 % RH and 1 vol.%

3.4.3. Accelerated carbonation under 90 % RH

Similar to the 70 % RH results for hydrated samples, there is a small amount (7 wc.%) of monosulfate formed during the first 6 h, which is then totally reacted at 24 h for hydrated specimens (Fig. 6 a)). However, ettringite is carbonated at the very beginning since a little vaterite and a reduction in ettringite are visible at 2 h. After 11 days of exposure, all the ettringite is depleted. The $CaCO_3$ polymorph and gypsum are essentially produced between 1 and 11 days. Strätlingite starts to react between 11 and 28 days, with no apparent change during the first 11 days of carbonation. An increase of Hc and monosulfate is identified at 11 and 28 days.

In the dehydrated samples (Fig. 6 b), ettringite reforms maximally around 15 wc.% and 8 wc.% for monosulfate. These two minerals are then totally depleted at 11 days. The pre-formed Hc is progressively consumed to 0 at 24 h. However, some Hc reforms after 11 and 28 days. Unlike in the hydrated samples, a steep decrease of strätlingite occurs at 11 days and a smaller depletion rate at 28 days. The total amounts of $CaCO_3$ and $CaSO_4$ in dehydrated samples are bigger than those in hydrated ones at 24 h, but being smaller at 11 days while no

difference is evident at 28 days. $CaCO_3$ appeared mainly at 24 h, while ettringite was detectable at the very beginning of experiments (2 h). This demonstrates that the rehydration of ettringite is faster than carbonation.

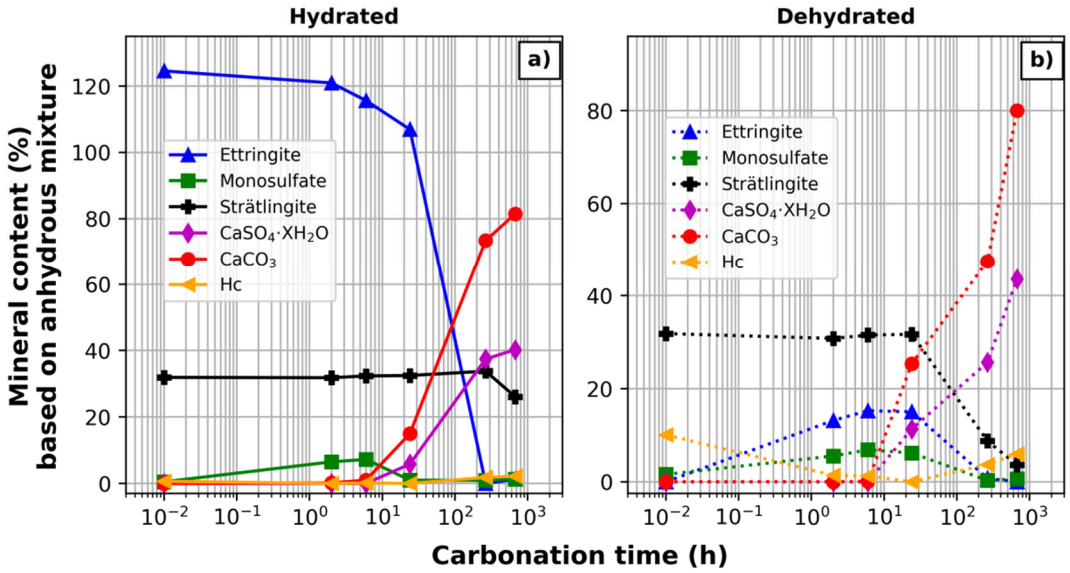

Figure 6. Calculated mineralogical contents in a) hydrated, and b) dehydrated C80P20 of 2–4 mm after different periods of accelerated carbonation under 90 % RH and 1 vol.%

3.5. Carbonation effect on TESC

Since C80P20 was the most resistant to CO_2 among the three binders, its TESC was investigated by TGA through samples with various quantities of bound CO_2 during accelerated carbonation at 70 % RH (Fig. 7). With reference to the fact that carbon can decompose ettringite irreversibly, it is expected that carbonation yields a decrease of TESC by depleting ettringite. Indeed, in this investigation, the TESC of the 1–2 mm samples reduces with carbonation underway. However, the initial growth of CO_2 binding quantity does not significantly reduce TESC when the CO_2 binding capacity is in the 0–0.075 range. The values stabilise at 880 ~ 890 J/g of anhydrous mixture, after which the TESC drops with an increase in the amount of bound CO_2. For carbonated 2–4 mm samples, the TESC was consistent with the 1–2 mm sample results.

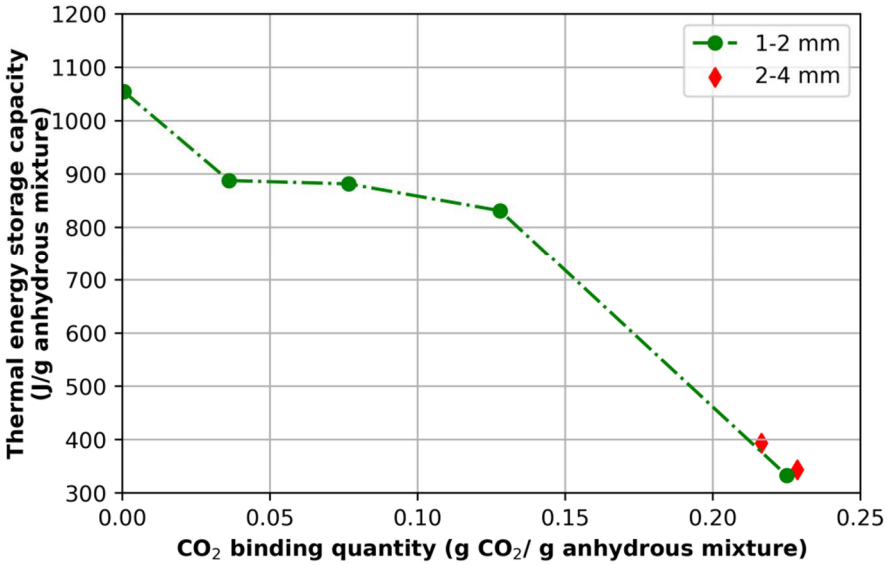

Figure 7. Thermal energy storage capacity of C80P20 as a function of CO_2 binding quantity at 70 % RH and 1 vol.% CO_2

4. Discussion

This work studies the carbonation of cement-based materials rich in ettringite/meta-ettringite for potential thermal energy storage use. The evolution of ettringite and carbonate content is discussed, with a comparison of two other materials with high ettringite content. Although ettringite is a dominant phase in these materials, other hydrates like monosulfate, strätlingite, and calcium aluminate hydrates contribute against carbonation to protect ettringite. The influence of CO_2 on the capacity of energy storage is also examined.

4.1. Pore size distribution vs. carbonation

Pores with diameters less than 0.1 µm behave like water containers during carbonation. The behaviour of pores as water containers strongly relies on environmental RH, which will be discussed in Section 4.4. Furthermore, more than 60 % of the pores in the samples are larger than 0.1 µm in diameter (Fig. 1), which ensures an efficient mass transfer of gaseous species via diffusion. For high-ettringite cement pastes of big w/c, the total porosities increase after carbonation and pores, especially with diameters < 0.1 µm, become more coarse [14]. According to [34], ettringite crystals tend to grow (directed or non-directed) in a direction less limited by solid pores, like into or around the pores rather than within the intrinsic solid matrix. This growth of crystals in solid pores can significantly decrease the diameter of micro pores but have less size influence for pores > 0.05 µm. This may explain how the increase of

ettringite content in cement pastes could reduce not only the size but also the volume of pores. Besides, ettringite crystals experienced a considerable change of **a** and **c** lattice parameters, which led to a decrease in crystal volume after dehydration [2]. Thus, the size and volume of ettringite-containing pores could be enlarged. Once the ettringite in the pores ($d < 0.05$ µm) is carbonated, the pores are going to be enlarged. However, the microstructure could be influenced by pre-treatments in a complex way, like during hydration, drying, or pre-carbonation [35]. Finally, MIP cannot quantify all types of pores, which leads to the implication that total porosity is higher.

4.2. Comparison of carbonation resistance for three binders

Among the three hydrated cement pastes that sustained accelerated carbonation, C60P40 seemed to be the least resistant against CO_2. This may be somewhat explained by the high calcium silicates' (C_3S and C_2S) content in anhydrous cement yielding C-S-H, which is more reactive to CO_2 than ettringite. Because of similar quantities of calcium silicates, the carbonation rate of BCSAF sample is comparable with that of C60P40 at an early stage of carbonation. The higher content of ettringite (hydrated) and meta-ettringite (dehydrated) in the C60P40 sample than the BCSAF makes C60P40 bind more CO_2 at 11 days. However, the BCSAF sample yields a higher theoretical CO_2 binding capacity than the C60P40 sample. The reduction of carbonation rate is therefore not as significant as in C60P40. Even the CO_2 binding quantity of BCSAF keeps approximately the same slope from 1 to 28 days, due to the logarithmic scale of time axis in Fig. 2, while the carbonation rate decreases. The same explanation is applicable for the C80P20 case. Additionally, C80P20 seems to present a lower CO_2 binding quantity and carbonation rate than the other two binders in both hydration states. It was thus the most resistant against CO_2, while C60P40 was the most easily carbonated in this investigation.

4.3. Effect of grain size on carbonation

As demonstrated in Fig. 3, at an appropriate RH (70 %), the small size leads to a higher carbonation degree after 24 h of carbonation. However, the visible differences in results between the samples of different sizes occur at 70 % RH. The influence of size is not observed for low RH (50 %) and high RH (90 %), which may be due to the lack of water supply at 50 % RH, bringing about a too-slow reaction. On the contrary, 90 % RH has a very high carbonation rate. This indicates that the effect of particle size may be controlled by RH and CO_2 concentrations, which could influence the dissolution rate of CO_2. At high RH and low RH, the process of equilibrium of water absorption has little influence on carbonation.

However, at 70 % RH, the process of water exchange between pore solution and humid air is significant. Note that the effect of size is more pronounced for dehydrated samples, the largest grain being slower to carbonate at an intermediate age, because achieving water sorption equilibrium needs more time for larger sized grains. Therefore, the carbonation is more significant at this RH.

4.4. Influence of RH

Carbonation of cementitious materials essentially depends on environmental RH [36,37]. Galan et al. [38] indicated that carbonation was affected by condensation of water in pores for OPC. 1) Firstly, the lack of water in pores at low humidity to dissolve reactants makes carbonation very slow, and 2) At intermediate RH, i.e., 50–70 % RH, there is enough water and diffusion space for CO_2 to accelerate carbonation, while a higher RH reduces carbonation speed because water saturation in pores slows it down. This saturation phenomenon may only be suitable for pores of small scale, where saturation of water can block the diffusion of CO_2. In this work, the carbonation of hydrated C80P20 grains (very porous) demonstrates that the higher the RH percentage, the higher the indicator of carbonation. This could be explained by the large porosity contributed by pores with diameters greater than 0.1 µm in samples. With a porosity of 34 % and the presence of pores > 0.1 µm, the transmission of water vapour and CO_2 is assumed to be too fast for the typical diffusion-controlled phenomenon.

Water content is key for determining the rate with a constant CO_2 concentration. At 50 % RH, the lack of pore solution limits the dissolution of CO_2, while at 90 % RH, a sufficient water content makes the CO_2 concentration the decisive factor of carbonation. When RH keeps at adequate values of 70 %, the equilibrium of water sorption makes the size effect on carbonation visible. This process needs time (the induction period was typically several hours in this study) to achieve the formation of ettringite-saturated pore solution and dissolution equilibrium of CO_2. Typically, the CO_2 binding quantities of hydrated C80P20 at 70 % RH are almost 5 times larger than the ones in samples of the same period at 50 % RH. At 90 % RH, the CO_2 binding quantities are bigger than those at 70 % RH, although the filling rate of pore solution is higher at 90 % RH (Table 5). Moreover, the generally low pore-filling rate as well as the high fraction of large pores can ensure good transport of CO_2. The large pore volume contributed by pores > 0.1 µm in C80P20 samples of both hydration states could still lead to an intense carbonation reaction with abundant water supply. Additionally, the average carbonation rate of dehydrated C80P20 between 6 and 24 h is found to be higher than that of the hydrated one at 90 % RH. This is due to carbonation being reinforced along with the

reformation of ettringite under high RH. It should be noted that in general, carbonation rate reduces with time. Between 11 and 28 days, the carbonation degree increases significantly more slowly than before, and tends to flatten for both 70 % and 90 % RH.

Table 6 Liquid saturation degree of pores by absorbed water for dry hydrated C80P20 using Eq. 6

RH (%)		55 ± 5	75 ± 5	95 ± 5
Liquid saturation degree (%)	1–2 mm	1.0	1.8	9.2
	2–4 mm	2.2	3.1	9.3

4.5. Influence of CO_2 concentration

The accelerated carbonation under 50 % RH with 1 vol.% CO_2 for hydrated 1–2 mm C80P20 (Fig. 3 a) is indeed more rapid than natural carbonation for each period because of the CO_2 concentration being 25 times greater. The hydrated samples are carbonated 5 times faster than dehydrated ones with 1 vol.%, while the difference is not significant for natural carbonation. Besides, the carbonation time of hydrated samples to bind with the same amount of CO_2 is approximately 45 times shorter under accelerated carbonation than natural carbonation. However, the difference of carbonation time is only approximately three times shorter for dehydrated samples. Considering the results in Fig. 3, the storage of C80P20 materials under ambient conditions (20 °C and 50 % RH) makes C80P20 materials of both hydration states reach less than 1 % carbonation degree for 6 months, which will not cause a significant carbonation problem.

4.6. Phase assemblage and reaction path

4.6.1. 50 % RH results

The general outline of TGA results are consistent with the evolution of components clarified by XRD. At 50 % RH, the very slight changes in quantity of carbonates in XRD proved the small increase of TGA curves. Due to the lack of water in dehydrated C80P20 samples, Hc exists during the entire investigation. Besides, the continuous slight increase of CO_2 bonding quantity in TGA cannot be directly confirmed by the increase of carbonation products in XRD. The explanation may be that, on the one hand the detection limit of XRD is not able to indicate the other carbonates, while on the other hand, some CO_3^{2-} substituted minerals exist in relatively low carbonated samples, which are not indistinguishable by XRD, like partially CO_3^{2-} substituted ettringite [2,39,40]. Moreover, the miscibility of CO_3^{2-} in SO_4-

519 ettrignite could be up to 60 % in the ettringite solid solution [26,27]. According to the
520 independent thermodynamic models in [1,41], ettringite may decompose to monosulfate (12-
521 hydrate) at low humidity because of a shift of equilibrium with water activity. This may
522 explain the reformation of monosulfate containing 12 H_2O in hydrated and dehydrated
523 C80P20 samples.

524 It is worth noting that the reformed "ettringite" in dehydrated samples may be a low-
525 hydrate ettringite with less than 30 H_2O, which is given by its wide peak of low intensity in
526 XRD patterns for 50 % RH cases in Fig. 8. According to [1], the reformed ettringite at
527 approximately 60 % RH presented wide and low counts peaks, which meant the minerals had
528 short-range order, and were not real crystals with long-range order. Thus, it could be a higher
529 hydration degree hydrate (12-hydrate meta-ettringite [1]) with respect to the initial meta-
530 ettringite.

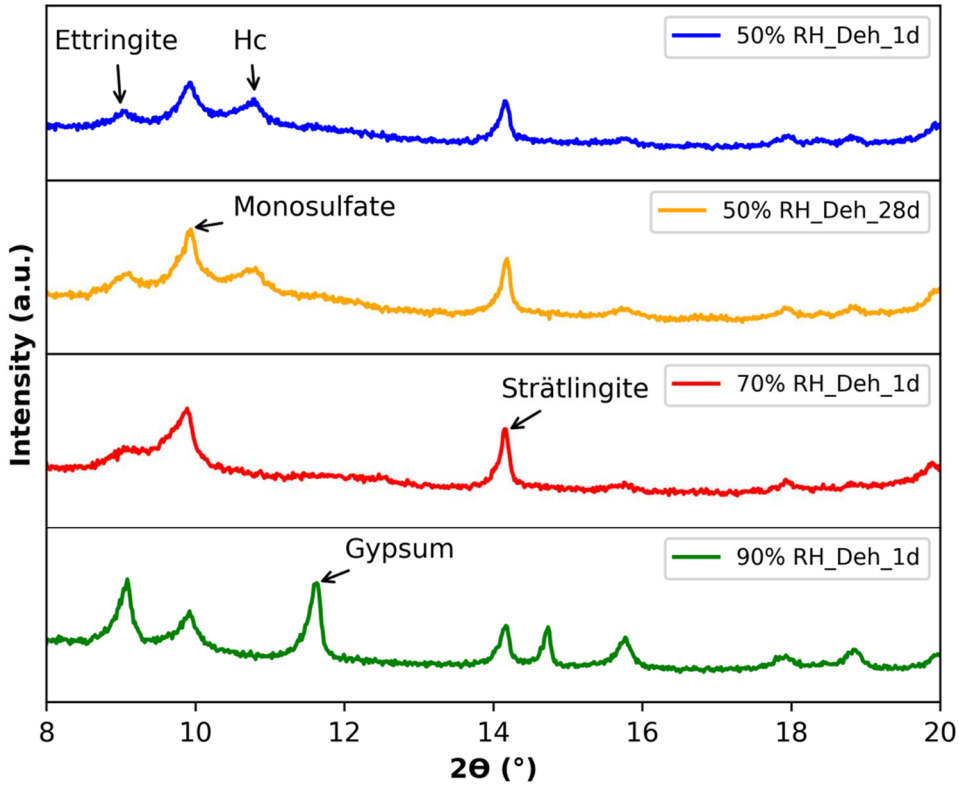

531

532 **Figure 8. XRD patterns of formed ettringite in dehydrated C80P20 grains of 2–4 mm at different**
533 **dates of carbonation in 1 % CO_2**

534 ### 4.6.2. 70 % RH results

535 When RH increases to 70 %, carbonation is significantly accelerated. Comparing TGA
536 (Fig. 3) with XRD (Fig. 5) results, all the slope break points correspond to the beginning of

carbonation of ettringite in hydrated samples and reformed ettringite in dehydrated samples, yielding carbonates and calcium sulphate hydrates. The oven-drying preparation with air circulation carbonates the samples and capture some CO_2, resulting in Hc in the dehydrated samples.

A certain amount of gypsum ($CaSO_4 \cdot 2H_2O$) is produced at 11 days for hydrated samples, while major hemihydrate ($CaSO_4 \cdot 0.5H_2O$) and trace gypsum is present after 28 days of carbonation. Ndiaye et al. [4] found hemihydrate instead of gypsum in an accelerated carbonation of 28 days at 65 % RH for an ettringite-based material. However, the survey [19] on accelerated carbonation (pure CO_2 gas) of a pure ettringite pellet at 68 % RH demonstrated the co-existence of these two calcium sulphate hydrates. Given that the direct transformation from $CaSO_4 \cdot 2H_2O$ to $CaSO_4 \cdot 0.5H_2O$ strictly needs high temperature and low RH [42], the authors assume that the carbonation leads a nucleation and crystallisation of hemihydrate from a saturated solution due to a local pH and water environment change. Carbonation has actually been reported to increase not only the porosity but also the size of pores [43], especially for gel pores (0.5–10 nm) and capillary pores (10 nm–10 µm). At an early age, water in micro pores (non-evaporable) plays a role in providing a very humid local environment to ensure producing a calcium sulphate di-hydrate. As carbonation proceeds, the collapse of ettringite crystal increases the amount and size of pores and porosity, making the water in pores evaporable. The exchange of water between materials and the environment is important, and the formed oversaturated pore solution forces crystallisation of lower hydrate degree minerals as hemihydrate with respect to gypsum. In the case of dehydrated samples, the lack of water caused by the hydration of dehydrated minerals makes that hemihydrate the only hydrate of calcium sulphate.

From TGA, it is seen that the binding of CO_2 at 70 % RH was more important than it was under 50 % RH. However, the effective diffusivity of CO_2 (0.8 ~ 1.8 vol.%) has no apparent change for high w/c hydrated cement paste at 47–78 % RH [35]. It is then rational to presume that on the one hand, a higher RH makes more water condensed in pores to dissolve CO_2, while on the other hand, the bigger consumption of carbonate ions in the solution at 70 % RH promotes local CO_2 dissolution in water.

4.6.3. 90 % RH results

At 90 % RH, carbonation is still accelerated compared to the results at 70 % RH. High water supplies and large porosity contributed by pores with diameters greater than 1 µm

favour the binding of CO_2 in the samples. Thus, the slope break point is advanced to 6 h (Fig. 3), and the ettringite and reformed ettringite in samples are totally consumed at 11 d. The reformed ettringite in dehydrated samples exhibiting a narrow and high counts peak in Fig. 7 suggests a good crystal structure and a higher rate of hydration than carbonation. According to [1], meta-ettringite could be hydrated to a 30-hydrate ettringite at 90 % RH. Therefore, the carbonation of meta-ettringite is actually acting on the reformed ettringite rather than on meta-ettringite with sufficient water supplies. Moreover, the carbonation rate of dehydrated samples younger than one day is indeed higher than the one of hydrated samples, which can be ascribed to the promotion effect by water. It can result in a higher rate of carbonation for dehydrated samples. At 11 days, the quantity of calcium sulphate hydrates in dehydrated samples is smaller than it is in hydrated samples. This indicates that a part of meta-ettringite is still somehow not carbonated. This meta-ettringite may lead to a local high pH solution once it is hydrated. Moreover, Hc was formed during the conversion of ettringite with reactive carbonates. Note that the final calcium sulphate in samples of both hydration states is proved to be gypsum, which is also indicated in [16,17] at RH superior than 90 %. Meantime aragonite and vaterite are the observed calcium carbonate polymorphs rather than calcite as reported in most investigations [16–18] on carbonation of pure ettringite. Strätlingite is supposed to get carbonated after the disappearance of ettringite and yield vaterite and aragonite as calcium carbonate polymorphs.

4.7. TESC vs. CO_2 binding quantity

The first decrease of TESC samples is due to ettringite not being dominant in getting carbonated. This protection may come from not only other hydrates in the samples like monosulfate and CSH, which are carbonated at higher rate than the one of ettringite, but also the possible formation of partial carbonate substituted ettringite. The miscibility of carbonate and sulphate ions could be up to 60 % without influence the number of water molecule [26–28]. Once ettringite begins to get carbonated, the reduction of TESC is assumed to be proportional to the increase of the quantity of bound CO_2. Specially, when the CO_2 binding quantity is greater than 0.13, the TESC decreased approximately 5000 J/g bound CO_2 (slope of curve) per gram of anhydrous C80P20 mixture. Moreover, no effect of grain size is observed during carbonation. For samples of different sizes with a CO_2 binding quantity of approximately 0.22, the TESCs are approximately 320 J/g of anhydrous mixture. Although the CO_2 binding quantity approaches the maximal value of 0.25, the rest of non-carbonated minerals and absorbed water are expected to contribute a certain capacity of storing energy. In

602 order to adapt to a real-world scale of application for storing thermal energy, the carbonation
603 kinetics of meta-ettringite enriched materials during usage cycles of hydration by cold humid
604 air and dehydration by hot dry air need to be further examined in a fixed bed reactor for
605 C80P20 samples [44]. Besides, with respect to the value of 1581 J/g $_{3CaO\cdot Al2O3\cdot 3CaSO4}$ adapted
606 from [1] for pure ettringite, the TESC of C80P20 (1054 J/g of anhydrous mixture) is indeed
607 lower due to relatively low ettringite content in composite material and carbonation influence.

608 ## 5. Conclusion

609 This study significantly advances the understanding of natural and accelerated carbonation
610 of ettringite and meta-ettringite-based material. The current results of carbonation
611 experimentations typically conducted by TGA and XRD lead to the following conclusions.

612 1. Relative humidity is the key controlling factor of carbonation, whatever the grain size
613 (1 to 4 mm) of ettringite and meta-ettringite-based materials. Both the instantaneous
614 rate of carbonation and the maximum degree of carbonation (up to 80 %) are
615 monotonic functions of relative humidity (up to 90 %).
616 2. Among the three mixtures investigated, C80P20 possesses a better carbonation
617 resistance than C60P40 and BCSAF thanks to a relatively lower porosity and high
618 ettringite content.
619 3. The ettringite-based material (hydrated C80P20) undergoes carbonation relatively
620 slowly at 50 % RH, while higher RH can accelerate carbonation. As for meta-
621 ettringite-based materials (dehydrated C80P20), carbonation occurs after hydration,
622 even if it is a low-hydrate ettringite of less than 30 H_2O at low RH. Conversely, 90 %
623 RH hydrates meta-ettringite into crystal ettringite and carbonates as fast as ettringite,
624 given that the hydration process of meta-ettringite is very fast under such RH.
625 4. For all samples of C80P20 in a natural environment (50 % RH), carbonation is a very
626 slow process. After exposure of 6 months, the hydrated and dehydrated C80P20
627 materials are carbonated to approximately 6 %. In contrast, the significant CO_2
628 binding quantity at 90 % RH and 1 vol.% CO_2 of C80P20 samples at 28 days indicates
629 that after release of heat via hydration by humid air, there is strong indication for the
630 material to be stored at low RH (< 50 % RH) or CO_2 free environment aiming at
631 avoiding the carbonation of ettringite and extending service life.
632 5. The $CaCO_3$ polymorphs formed after carbonation of ettringite and meta-ettringite are
633 confirmed as vaterite and aragonite, while the final polymorph of $CaSO_4$ is
634 hemihydrate at 70 % RH and gypsum at 90 % RH.

6. The reduction of ettringite content caused by carbonation indeed decreases the thermal energy storage capacity of C80P20. When the CO_2 binding quantity is 0.035–0.075, it could store approximately 890 J/g of anhydrous material. Further loss of energy storage capacity is observed with deepening of the carbonation of C80P20.

6. Acknowledgement

The authors would like to thank LafargeHolcim Innovation Center and Association Nationale de la Recherche et de la Technologie (ANRT) of France for the funding of this research. The authors address the appreciation to Mouna Boumaaza, Isabelle Baco and the analytical support team from LafargeHolcim Innovation Center for their precious discussions and analysis support.

7. References

[1] L.G. Baquerizo, T. Matschei, K.L. Scrivener, Impact of water activity on the stability of ettringite, Cem. Concr. Res. 79 (2016) 31–44. doi:https://doi.org/10.1016/j.cemconres.2015.07.008.

[2] B. Chen, F. Kuznik, M. Horgnies, K. Johannes, V. Morin, E. Gengembre, Physicochemical properties of ettringite/meta-ettringite for thermal energy storage: Review, Sol. Energy Mater. Sol. Cells. 193 (2019) 320–334. doi:https://doi.org/10.1016/j.solmat.2018.12.013.

[3] L.J. Struble, P.W. Brown, Heats of dehydration and specific heats of compounds found in concrete and their potential for thermal energy storage, Sol. Energy Mater. 14 (1986) 1–12. doi:https://doi.org/10.1016/0165-1633(86)90008-0.

[4] K. Ndiaye, M. Cyr, S. Ginestet, Durability and stability of an ettringite-based material for thermal energy storage at low temperature, Cem. Concr. Res. 99 (2017) 106–115. doi:https://doi.org/10.1016/j.cemconres.2017.05.001.

[5] J. Kaufmann, F. Winnefeld, Seasonal heat storage in calcium sulfoaluminate based hardened cement pastes – experiences with different prototypes, J. Energy Storage. 25 (2019).

[6] J. López-Beceiro, C. Gracia-Fernández, J. Tarrío-Saavedra, S. Gómez-Barreiro, R.

664 Artiaga, Study of gypsum by PDSC, J. Therm. Anal. Calorim. 109 (2012) 1177–1183.
665 doi:10.1007/s10973-012-2335-1.

666 [7] P. Pardo, A. Deydier, Z. Anxionnaz-Minvielle, S. Rougé, M. Cabassud, P. Cognet, A
667 review on high temperature thermochemical heat energy storage, Renew. Sustain.
668 Energy Rev. 32 (2014) 591–610. doi:https://doi.org/10.1016/j.rser.2013.12.014.

669 [8] K. Ndiaye, S. Ginestet, M. Cyr, Thermal energy storage based on cementitious
670 materials: A review, AIMS Energy. 6 (2018) 97–120.
671 doi:http://dx.doi.org/10.3934/energy.2018.1.97.

672 [9] J. Kaufmann, F. Winnefeld, Cement-based chemical energy stores, 2011.

673 [10] M. Cyr, S. Ginestet, K. Ndiaye, Energy storage/withdrawal system for a facility, 2015.

674 [11] Y.F. Houst, Diffusion de gaz, carbonatation et retrait de la pâte de ciment durcie, EPFL
675 PP - Lausanne, 1992. doi:10.5075/epfl-thesis-1108.

676 [12] B. Šavija, M. Luković, Carbonation of cement paste: Understanding, challenges, and
677 opportunities, Constr. Build. Mater. 117 (2016) 285–301.
678 doi:10.1016/j.conbuildmat.2016.04.138.

679 [13] J.-M. Mechling, A. Lecomte, A. Roux, B. Le Rolland, Sulfoaluminate cement
680 behaviours in carbon dioxide, warm and moist environments, Adv. Cem. Res. 26 (2014)
681 52–61. doi:10.1680/adcr.12.00070.

682 [14] C.W. Hargis, B. Lothenbach, C.J. Müller, F. Winnefeld, Carbonation of calcium
683 sulfoaluminate mortars, Cem. Concr. Compos. 80 (2017) 123–134.
684 doi:https://doi.org/10.1016/j.cemconcomp.2017.03.003.

685 [15] V.G. Papadakis, M.N. Fardis, C.G. Vayenas, Effect of composition, environmental
686 factors and cement-lime mortar coating on concrete carbonation, Mater. Struct. 25
687 (1992) 293–304. doi:10.1007/BF02472670.

688 [16] T. Nishikawa, K. Suzuki, S. Ito, K. Sato, T. Takebe, Decomposition of synthesized
689 ettringite by carbonation, Cem. Concr. Res. 22 (1992) 6–14.
690 doi:https://doi.org/10.1016/0008-8846(92)90130-N.

691 [17] T. Grounds, H. G Midgley, D. V Novell, Carbonation of ettringite by atmospheric

carbon dioxide, Thermochim. Acta. 135 (1988) 347–352. doi:https://doi.org/10.1016/0040-6031(88)87407-0.

[18] X. Chen, R. Zou, X. Chen, Kinetic study of ettringite carbonation reaction, Cem. Concr. Res. 24 (1994) 1383–1389. doi:https://doi.org/10.1016/0008-8846(94)90123-6.

[19] Q. Zhou, F.P. Glasser, Kinetics and mechanism of the carbonation of ettringite, Adv. Cem. Res. 12 (2000) 131–136. doi:10.1680/adcr.2000.12.3.131.

[20] I. Pajares, S. Martínez-Ramírez, M.T. Blanco-Varela, Evolution of ettringite in presence of carbonate, and silicate ions, Cem. Concr. Compos. 25 (2003) 861–865. doi:https://doi.org/10.1016/S0958-9465(03)00113-6.

[21] D. Zhang, D. Xu, X. Cheng, W. Chen, Carbonation resistance of sulphoaluminate cement-based high performance concrete, J. Wuhan Univ. Technol. Sci. Ed. 24 (2009) 663–666. doi:10.1007/s11595-009-4663-y.

[22] S. Ioannou, L. Reig, K. Paine, K. Quillin, Properties of a ternary calcium sulfoaluminate-calcium sulfate-fly ash cement, Cem. Concr. Res. 56 (2014) 75–83. doi:10.1016/j.cemconres.2013.09.015.

[23] S. Ioannou, K. Paine, L. Reig, K. Quillin, Performance characteristics of concrete based on a ternary calcium sulfoaluminate-anhydrite-fly ash cement, Cem. Concr. Compos. 55 (2015) 196–204. doi:10.1016/j.cemconcomp.2014.08.009.

[24] J. V Brien, K.R. Henke, K.C. Mahboub, Influence of latex polymer addition on the behavior of materials containing CSA cement cured at low humidity, J. Green Build. 8 (2013) 94–109. doi:10.3992/jgb.8.4.94.

[25] L. Zhang, F.P. Glasser, Investigation of the microstructure and carbonation of CSA-based concretes removed from service, Cem. Concr. Res. 35 (2005) 2252–2260. doi:https://doi.org/10.1016/j.cemconres.2004.08.007.

[26] H.-J. Pöellmann, H., Kuzel, Solid solution of ettringites Part1: Incorporation of OH- and CO32- in 3CaO·Al203·3CaSO4·32H20, Cem. Concr. Res. 20 (1990) 941–947.

[27] S.J. Barnett, C.D. Adam, A.R.W. Jackson, An XRPD profile fitting investigation of the solid solution between ettringite, Ca6Al2(SO4)3(OH)12·26H2O, and carbonate ettringite, Ca6Al2(CO3)3(OH)12·26H2O, Cem. Concr. Res. 31 (2001) 13–17.

721 doi:https://doi.org/10.1016/S0008-8846(00)00429-4.

722 [28] T. Matschei, B. Lothenbach, F.P. Glasser, Thermodynamic properties of Portland
723 cement hydrates in the system CaO–Al2O3–SiO2–CaSO4–CaCO3–H2O, Cem. Concr.
724 Res. 37 (2007) 1379–1410. doi:https://doi.org/10.1016/j.cemconres.2007.06.002.

725 [29] K. Quillin, Performance of belite-sulfoaluminate cements, Cem. Concr. Res. 31 (2001)
726 1341–1349. doi:10.1016/S0008-8846(01)00543-9.

727 [30] E. Gartner, H. Hirao, A review of alternative approaches to the reduction of CO2
728 emissions associated with the manufacture of the binder phase in concrete, Cem. Concr.
729 Res. 78 (2015) 126–142. doi:https://doi.org/10.1016/j.cemconres.2015.04.012.

730 [31] H.F.W. Taylor, Cement chemistry, 2nd., Thomas Telford, London, 1997.

731 [32] M. Thiery, P. Dangla, P. Belin, G. Habert, N. Roussel, Carbonation kinetics of a bed of
732 recycled concrete aggregates: A laboratory study on model materials, Cem. Concr. Res.
733 46 (2013) 50–65. doi:https://doi.org/10.1016/j.cemconres.2013.01.005.

734 [33] L. Greenspan, Humidity fixed points of binary saturated aqueous solutions, J. Res. Natl.
735 Bur. Stand. (1934). 81 (1977) 89–96.

736 [34] S. Chinchón-Payá, A. Aguado, S. Chinchón, A comparative investigation of the
737 degradation of pyrite and pyrrhotite under simulated laboratory conditions, Eng. Geol.
738 127 (2012) 75–80. doi:10.1016/j.enggeo.2011.12.003.

739 [35] Y.F. Houst, F.H. Wittmann, Influence of porosity and water content on the diffusivity
740 of CO2 and O2 through hydrated cement paste, Cem. Concr. Res. 24 (1994) 1165–
741 1176. doi:https://doi.org/10.1016/0008-8846(94)90040-X.

742 [36] Y.F. Houst, The role of moisture in the carbonation of cementitious materials, Int.
743 Zeitschrift Für Bauinstandsetz. Und Baudenkmalpfl. 2 (1996) 49–66.

744 [37] M. Boumaaza, B. Huet, G. Pham, P. Turcry, A. Aït-Mokhtar, C. Gehlen, A new test
745 method to determine the gaseous oxygen diffusion coefficient of cement pastes as a
746 function of hydration duration, microstructure, and relative humidity, Mater. Struct. 51
747 (2018) 51. doi:10.1617/s11527-018-1178-z.

748 [38] I. Galan, C. Andrade, M. Castellote, Natural and accelerated CO2 binding kinetics in

749 cement paste at different relative humidities, Cem. Concr. Res. 49 (2013) 21–28.
750 doi:https://doi.org/10.1016/j.cemconres.2013.03.009.

751 [39] F.P. Glasser, The stability of ettringite, in: Int. RILEM Work. Intern. Sulfate Attack
752 Delayed Ettringite Form., RILEM Publications SARL, 2002: pp. 43–64.

753 [40] F. Winnefeld, C. Hargis, S. Steiner, J. Kaufmann, A. Borgschulte, M. Marchi, S. Allevi,
754 B. Lothenbach, Carbonation resistance of calcium sulfoaluminate cement mortars, in:
755 Conf. to Celebr. Centen. LMC Karen Scrivener's 60th Birthd., Lausanne, Switzerland,
756 2018: pp. 243–246.

757 [41] B. Albert, B. Guy, D. Damidot, Water chemical potential: A key parameter to
758 determine the thermodynamic stability of some hydrated cement phases in concrete?,
759 Cem. Concr. Res. 36 (2006) 783–790. doi:10.1016/j.cemconres.2005.12.016.

760 [42] J.R. Clifton, Thermal analysis of calcium sulfate dihydrate and sopposed alpha and beta
761 forms of calcium sulfate hemihydrate from 25 to 500 °C, J. Res. Natl. Bur. Stand. - A.
762 Phys. Chemmistry. 76 A (1972) 41–49.

763 [43] V. Shah, K. Scrivener, B. Bhattacharjee, S. Bishnoi, Changes in microstructure
764 characteristics of cement paste on carbonation, Cem. Concr. Res. 109 (2018) 184–197.
765 doi:https://doi.org/10.1016/j.cemconres.2018.04.016.

766 [44] B. Chen, F. Kuznik, M. Horgnies, K. Johannes, V. Morin, E. Gengembre, A Modular
767 Reactor for Thermochemical Energy Storage Examination of Ettringite-Based
768 Materials, Proceedings. 34 (2019) 18. doi:10.3390/proceedings2019034018.

769